ORIGINAL ARTICLE

Fault Impact Analysis and Improvements for a Large-scale Offshore Wind Farm Connected to Grid by Long HVAC Cables

Chia-Yu Han[1,*], Feng-Jih Wu[2], Chih-Ju Chou[3], and Ching-Yin Lee[4]

[1] *Center of Energy Economics and Strategy Research, Institute of Nuclear Energy Research, Atomic Energy Council, Taiwan*
[2] *Department of Electrical Engineering, St. John's University, New Taipei City 25135, Taiwan*
[3] *Department of Electrical Engineering, National Taipei University of Technology, Taipei 10608, Taiwan*
[4] *Department of Electrical Engineering, Tungnan University, New Taipei City 222, Taiwan*
(**Received** 27 November 2015; **Accepted** 1 January 2016; **Published on line** 1 June 2016)
*Corresponding author: s49130153@gmail.com
DOI: 10.5875/ausmt.v6i2.1080

Abstract: A large-scale offshore wind power system with a capacity 200MW will be erected in the Peng-Hu islands, located about 60 km off the west coast of Taiwan. The system will be connected to Taiwan's main grid by long high-voltage alternating-current (HVAC) submarine cables. The system impact of three phase short circuit faults are analyzed based on PSS/E simulations of type-B, C and D turbines. The system framework, associated parameters, and the features of different types of wind turbines are described. Responses of voltages, frequencies and powers of each turbine type due to fault disturbance are analyzed. In addition, the voltage and frequency variations of the Taiwan and Peng-Hu grids are compared in terms of different turbine types. Finally, improvements based on static VAr compensator (SVC) and static synchronous compensator (STATCOM) technologies are presented and their fault impact mitigation capacities are analyzed. Analysis results show that fault impact is significantly dependent on turbine type and the presented compensators provide useful impact mitigation.

Keywords: wind resource, High-Voltage Direct-Current (HVDC), greenhouse gases, submarine cable, PSS/E, fault ride through, Static VAr compensator (SVC), Static synchronous compensator (STATCOM)

Introduction

As part of efforts to reduce greenhouse gas emission, Taiwan is in the process of developing a large-scale offshore wind power project with an eventual maximum production capacity of 200MW. The development site is in the Peng-Hu Islands, about 60 km off Taiwan's west coast, as shown in Fig. 1. Electricity produced by the wind farm will be transmitted to Taiwan's main power grid through two high-voltage alternating-current (HVAC), 161kV submarine cables. Compensative reactors will be installed at both ends to compensate for capacitive charging currents. Unlike high-voltage direct-current (HVDC) links, HVAC links provide a high degree of coupling between two grids [1-4]. In addition, long HVAC cables with reactors will produce more complex transient characteristics especially during fault transient states. These factors will increase the severity of fault impacts on large capacity wind power systems, which are inherently more fault sensitive than smaller-capacity generating systems. Previous studies have examined fault impacts on wind power system [1, 2, 5, 6], finding that the dynamic performance of wind turbines were given with more attention than the interactions between the grid and wind turbines. Grids are frequently depicted as simplified models [5] to deal with problems related to the integration of large-scale wind power generation into electric power systems. This paper examines fault impacts on large-scale offshore wind power systems and grids, using a case study of an actual grid system, rather than a simplified model. This paper aims to analyze the most serious fault, namely three phase short circuit (3ΦSC) fault, and to assess its impact on wind turbines, and the Peng-Hu and Taiwan grids. Variations of voltages, frequencies, and power output due to fault disturbances

Copyright © 2016 International Journal of Automation and Smart Technology

are analyzed through engineering (PSS/E) simulations [7]. Three types of wind turbines are considered, and their respective configurations, performances and protective relays settings are described in detail. Simulation conditions and results for various turbine types are then compared. The benefits of integrating reactive compensation devices into the wind system are analyzed.

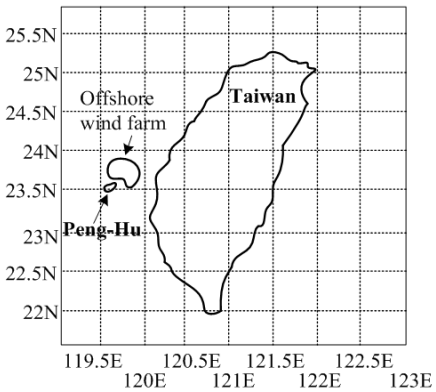

Figure 1. Location of Peng-Hu offshore wind farm.

System Description

System framework and parameters

The system framework comprises the offshore wind farm, the Peng-Hu grid, the HVAC submarine transmission system and the Taiwan grid and is represented as a single-line diagram shown in Fig. 2. The offshore wind farm is composed of eight groups of 20 wind turbines each, and each is interconnected to a common bus which is connected to the 33kV collection bus at secondary side of the set-up land-based transformer. The system includes four set-up transformers with ratings of 120MVA, with 33kV secondary and 161kV primary voltages. These transformers are connected in parallel to the 161kV main bus (Bus-03). Each transformer services two groups of wind turbine units. The total installation capacity is assumed to be 200MW. The HVAC transmission system consists of two submarine cables measuring 58.9km in length, with single cores and cross-sections of 600mm^2, a rated capacity of 200MW and a rated voltage of 161kV. As shown in Fig. 2, the Peng-Hu and Taiwan grids connect to the submarine cables by the 161kV buses, which are connected by transformers and part of buses to downstream substations. The 1,996 buses in the Taiwan grid are modeled in the PEE/S simulations. The submarine transmission system connects to the Taiwan grid through the 161kV bus (Bus-09) at the Tai-Zi substation, which is connected to the 161kV bus (Bus-05) of the upstream Kou-Hu substation by two 7.2km XLPE land cables (underground cables). On the Peng-Hu side, the submarine cables connected to Bus-04, which is then connected to two 0.3km land cables to the 161kV bus (Bus-03) at the wind farm. To meet grid code requirements, the reactors are installed on the bus at the connection to the submarine cables to compensate for the cables' capacitive reactive power.

Chia-Yu Han, he received the Ph.D. degree in National Taipei University of Technology (NTUT). He is currently an Associate Research & Development Engineer in Center of Energy Economics and Strategy Research, Institute of Nuclear Energy Research, Atomic Energy Council, Taiwan.

Feng-Jih Wu, he received the Ph.D. degree in NTUT. He is currently an Associate professor of electrical engineering in St. John's University.

Chih-Ju Chou, he received his M.S. degree in electrical engineering from National Taiwan Institute of Technology in 1986 and Ph.D. degree in electrical engineering from National Taiwan University, Taiwan in 1994. He has been with National Taipei University of Technology in Taiwan, where he is currently a professor of electrical engineering.

Ching-Yin Lee, he received the B.S.E.E. degree from National Taiwan Institute of Technology, Taipei, Taiwan, in 1983, the M.S.E.E. degree from National Taiwan University, Taipei, in 1986, and the Ph.D. degree from National Taiwan University of Science and Technology, Taipei, in 1992. He is currently an Honorable Professor at NTUT and a Professor and the President at Tungnan University, Taipei.

Features of different types of wind turbines

Wound rotor induction generators (WRIG) and permanent magnet synchronous generators (PMSG) are used with various power electronic topologies to form different types of wind turbines [5]. Three types of variable speed wind turbines are widely used, and are classified as types B, C and D [1]. Their respective configurations, performances and protective relay settings are described as follows.

Type-B wind turbine

Figure 3 shows the type-B wind turbine configuration [1]. A variable resistor in series with the WRIG rotor circuit is used to adjust the speed and air-gap torque. Usually, the variable resistor is changed by an optically controlled converter [1], and thus controlling the total resistance variation of the rotor circuit. To improve the starting performance and power factor, a soft-starter and reactive power compensation devices are usually required. A capacitor bank with a capacity of 0.9MVAr is used for reactive power compensation during simulations. Figure 4 shows the effect of varying the rotor resistance on the induction generator torque. This study is concerned with the generating region (i.e. region of negative slip and torque). Table 1 summarizes the settings of the protective relays [8]. The protective relays will be fast tripped when the voltage exceeds 1.2p.u. or falls below 0.75p.u. and when the frequency exceeds 62Hz or falls below 57Hz. Figure 5 plots the voltage protection for each wind turbine type, and the current fault ride-through capability (LVRT) of Taiwan Power Company (TPC).

Copyright © 2016 International Journal of Automation and Smart Technology

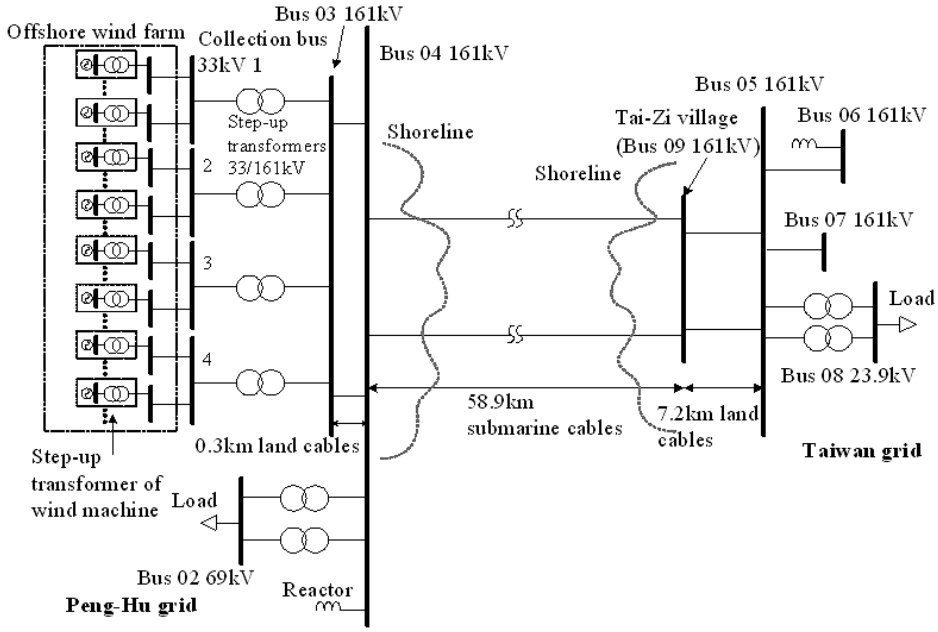

Figure 2. Single-line diagram depicting the offshore wind power system framework.

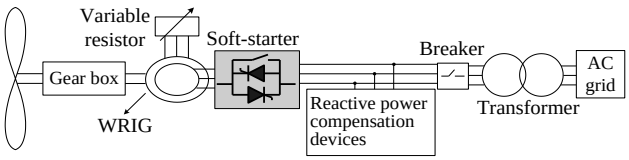

Figure 3. Type-B wind turbine configuration.

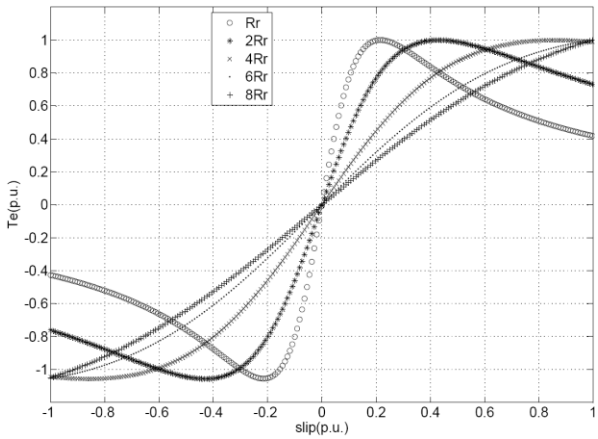

Figure 4. WRIG torque-slip curves with respect to various rotor circuit resistances.

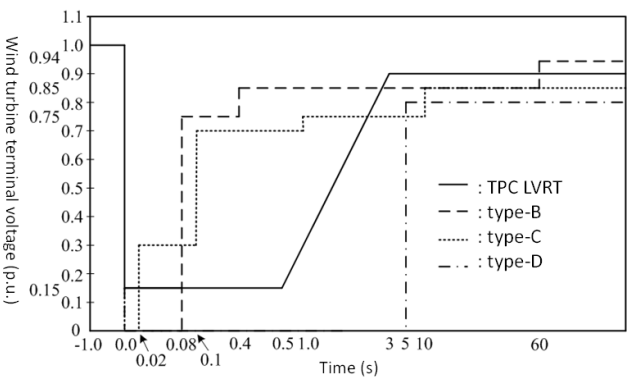

Figure 5. LVRT for each type of wind turbine and TPC's LVRT.

Type-C wind turbine

The type-C wind turbine is also called a doubly fed induction generator (DFIG) because power can be transmitted to the grid via a stator or rotor. In the configuration shown in Fig. 6, a partial-scale frequency converter is installed on the WRIG rotor circuit [1]. This converter not only performs reactive power compensation and provides a smoother grid connection, but also enables the turbine to operate at a unity power factor in over-synchronous or sub-synchronous operation modes depending on the generator's rotational speed. In over-synchronous mode, power will be transmitted from the rotor through the converters to the grid; in sub-synchronous mode, the rotor will absorb power from the network via the converters [1, 6]. The settings of the protective relays listed in Table 1 show that fast tripping will occur when voltage exceeds 1.3p.u. or falls below 0.3p.u. and when frequency exceeds 62.5Hz or falls below 56.5Hz [8]. These settings mean that the type-C wind turbine can tolerate more severe voltage and frequency variations than the type-B turbine.

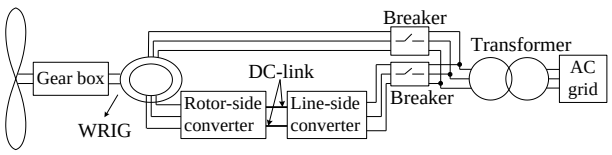

Figure 6. Type-C wind turbine configuration.

Type-D wind turbine

The type-D wind turbine is a full variable speed wind turbine. It may or may not include a gear box, and different type of generators can be employed, such as

Copyright © 2016 International Journal of Automation and Smart Technology

WRIG or PMSG, as shown in Fig. 7 [1]. The rotor of the generator is connected to the grid by a full-scale frequency converter and all of the power from the turbine goes through this converter; hence the dynamic operation of the generator is absolutely isolated from the grid. The type of power converter arrangement employed will influence the operation of the generator and the power flows to the grid. Each converter is able to generate or absorb reactive power independently [6]. The settings of the protective relays are listed in Table 1 [8]; type-D wind turbines do not need to fast trip to ensure under voltage protection. Compared with type-B and type-C turbines, the type-D wind turbine better withstands voltage and frequency variations.

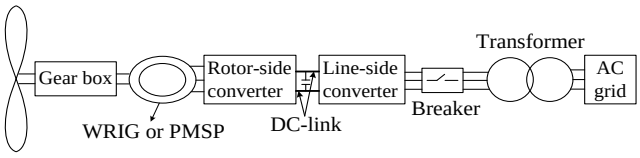

Figure 7. Type-D wind turbine configuration.

Analysis Cases and Results

The fault impact analysis simulates variations of voltage and frequency on the grid buses, as well as the terminal voltage, frequency, active power, reactive power and the pitch angle of the individual wind turbine due to the disturbance of 3ΦSC fault in the grid with off-peak load levels. The analysis is based on PSS/E simulations. In all simulations, the fault point is assumed to be on the Bus-03 as shown in Fig. 2, and all the wind turbines operate at a rated wind speed of 12m/s with rated power output. The rated power of individual type-B, C and D turbines are respectively 1.8MW, 3.6MW and 2.3MW, with total respective deployments of 112, 56 and 88 units. For the type-B turbines, a capacitor bank is connected to provide 0.9MVAr reactive power compensation, while type-C and type-D turbines are assumed to come under the unity power factor. However, to facilitate the simulations, each turbine is considered to operate under the same conditions, and thus the contribution of fault-current for each wind turbine is the same. The off-peak load level of the Taiwan grid is 21,708.46+*j*2,179.02MVA distributed over 580 load buses (not shown in Fig. 2). All the loads are modeled as constant current and constant admittance during the dynamic study. The power consumptions of loads connected to Bus-02 and Bus-08 in Fig. 2 are 35.8+*j*3.6MVA and 7.3+*j*0.7MVA, respectively. The buses observed in the simulation include Bus-02 and Bus-04 on the Peng-Hu grid and Bus-05 to Bus-08 on the

Table 1. Settings and pickup time of the protective relays for different.

Wind turbine types	Settings (p.u.) and pickup time(s) of voltage relay					Settings (Hz) and pickup time(s) of frequency relay				
	Continuous operation range	Under-voltage relay		Over-voltage relay		Continuous operation range	Under-frequency relay		Over-frequency relay	
Type-B	0.94-1.1	< 0.75	0.08	1.1-1.11	60	57-62	< 57	0.2	> 62	0.2
		0.75-0.85	0.4	1.11-1.135	0.08					
		0.85-0.94	60	1.135-1.2	0.2					
				> 1.2	0.08					
Type-C	0.85-1.1	< 0.3	0.02	1.1-1.15	1	57.5-61.5	< 56.5	0.02	> 62.5	0.02
		0.3-0.7	0.1	1.15-1.3	0.1					
		0.7-0.75	1	> 1.3	0.02		56.5-57.5	10	61.5-62.5	30
		0.75-0.85	10							
Type-D	0.8-1.2	< 0.8	5	1.2-1.45	5	57-62	< 57	0.06	> 62	0.06
				> 1.45	0.05					

Copyright © 2016 International Journal of Automation and Smart Technology

Taiwan grid (Fig. 2).

Figures 8-10 respectively show time domain variation curves covering the time from pre-fault to post-fault for type-B, C and D turbines. These figures are created automatically by PSS/E without ordinate unit markings because of several curves with different units are included in the same figure. In the figures, the fault begins at 2s and finishes (i.e., clears) at 2.1s.

In pre-fault and post-fault time intervals, the small differences in bus voltages between different turbine types are due to small differences of voltage drops. The transformer reactance for the type-B, C and D turbines are respectively 0.075p.u. based on 2MVA, 0.07p.u. based on 4MVA and 0.0375p.u. based on 2.5MVA. The reactance of the type-B turbine is slightly larger than that of the type-C turbine, however a capacitor bank is connected for reactive power compensation in the type-B turbine and thus its bus voltage exceeds that of the type-C case in pre-fault time intervals. Because the Peng-Hu grid buses (Bus-02 to 04) are very near the fault point, their voltage drops are much larger than those of the Taiwan grid buses (Bus-05 to 08) during fault. The terminal voltage of each turbine type is almost zero during fault, thus the under voltage relays of the type-B and type-C turbines will trip out (see Table 1). The under voltage relays of the type-D turbines, however, will not trip because of their pick-up time (5s) over fault duration (0.1s). In addition to the relay trip times listed in Table 1, the breaker time is also considered in the simulation. Consequently, type-B and type-C turbines will be respectively disconnected from system at the time points 2.16s and 2.1s. The trip out time of type-B wind turbines is delayed 0.06s after fault clearance

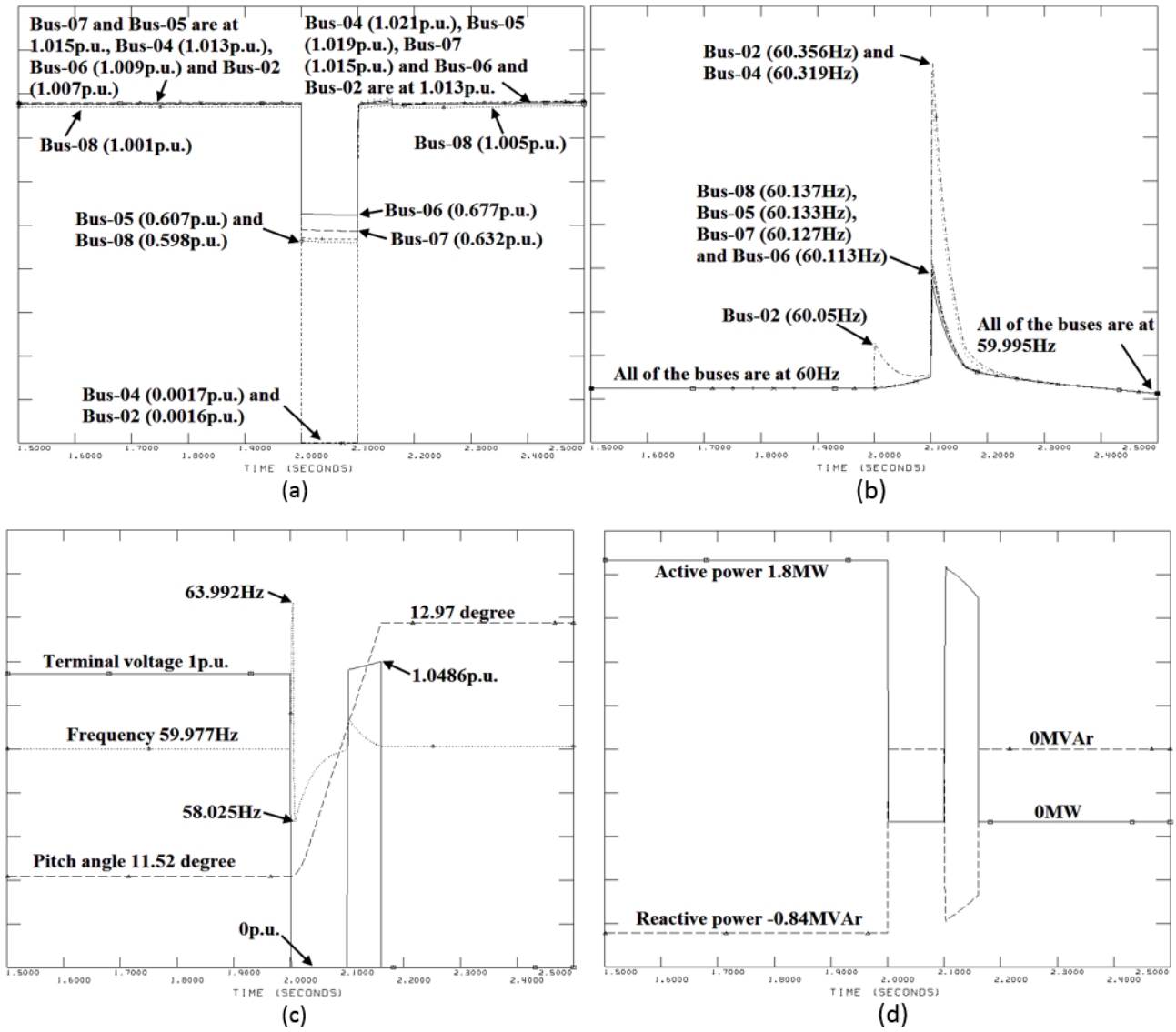

Figure 8. Simulation results for type-B turbine connected operation and fault on the Peng-Hu grid: (a) voltage and (b) frequency responses of the buses, (c) terminal voltage, frequency and pitch angle and (d) active and reactive power responses.

Copyright © 2016 International Journal of Automation and Smart Technology

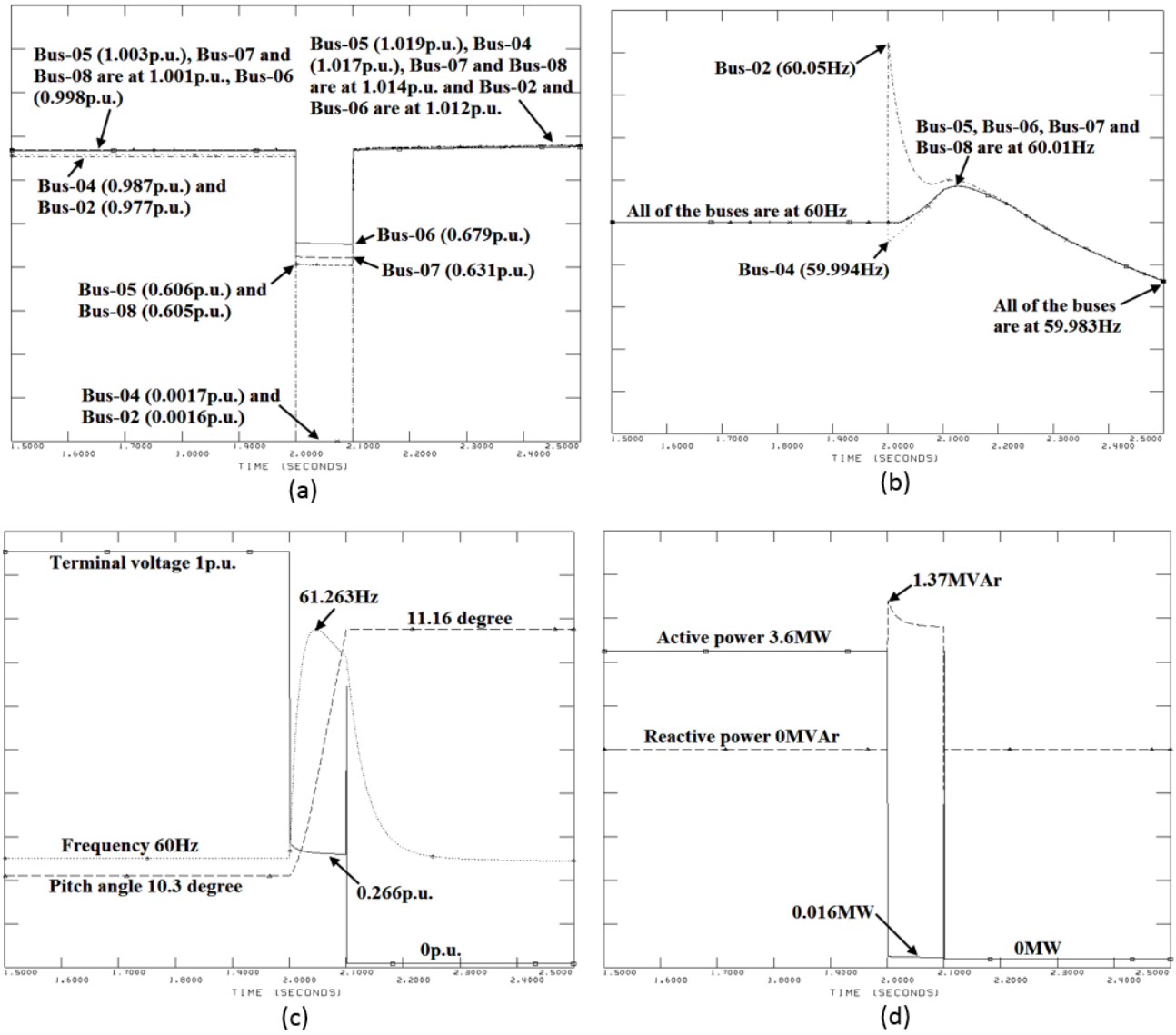

Figure 9. Simulation results for type-C turbine connected operation and fault on the grid of Peng-Hu (a) voltage and (b) frequency responses of the buses, (c) terminal voltage, frequency and pitch angle and (d) active and reactive power responses of the wind turbine.

(2.1s). For the same reason, the terminal voltage of the type-C wind turbine is recovered at the instant of fault clearance and then disconnected from the grid due to the breaker action. The fault also causes the type-D wind turbine to trip out at the instant of fault occurrence because of over-frequency relay action (see Fig. 10 (c) and Table 1).

As shown in Figs. 8(d) and 9 (d), the type-C wind turbine has a reactive power output of 1.36MVAr during the fault and sustains its terminal voltage at 0.27p.u., on the other hand, the type-D wind turbine temporarily switches off the IGBTs [9] to block the active power output at the generator side converter, thus reducing current output to zero; hence the active and reactive power are both zero during the fault. While the wind turbine is disconnected, the active and reactive power are maintained at zero after fault clearance.

Improvement Methods

The wind power penetration in the power system has growing to a high level relatively, thus reducing power system reliability and stability, and leaving the system vulnerable to unpredictable variations in the wind energy, which are particularly acute in isolated or island areas. To increase stability, wind turbine manufacturers have developed a new system to enhance fault ride through and provide active and reactive power control capability, such as DFIG and PMSG. Installing reactive power compensators in wind farms also helps reduce the impact of wind farm operations on the overall power system [6]. The benefits of integrating reactive power compensation devices such as static VAr compensator (SVC) and static synchronous compensator (STATCOM) in wind power

Copyright © 2016 International Journal of Automation and Smart Technology

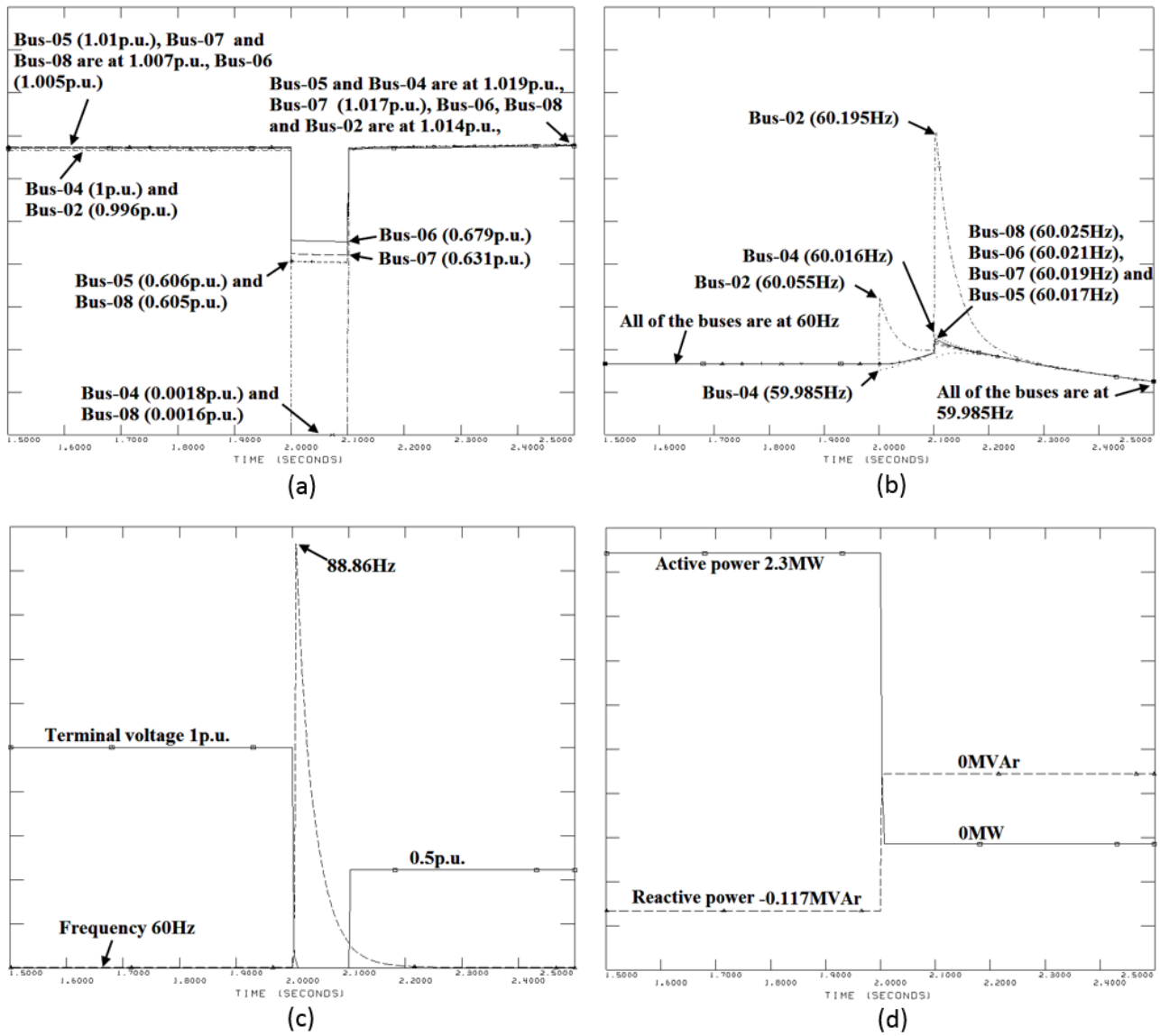

Figure 10. Simulation results for type-D turbine connected operation and fault on the Peng-Hu grid: (a) voltage and (b) frequency responses of the buses, (c) terminal voltage and frequency and (d) active and reactive power responses of the wind turbine.

generation system will be studied further. Figure 2 shows the Taiwan and Peng-Hu grid system, while Fig. 11 shows integration of the reactive power compensation devices. The simulation assumes that the capacity of SVC and STATCOM are both 100MVA and are installed on the 33kV collection bus to regulate the voltage at 1p.u. before the fault occurs. The fault is on Bus 03 and is applied at 2s and cleared at 2.1s.

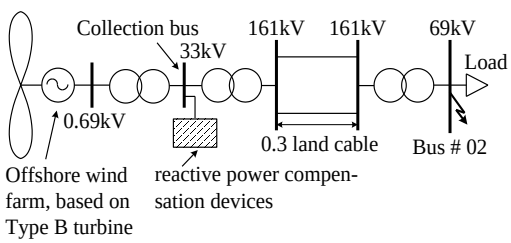

Figure 11. An offshore wind farm interconnected to the grid with reactive power compensation.

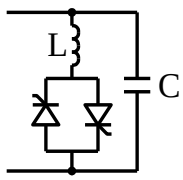

Figure 12. Thyristor-controlled reactor with a fixed capacitor.

Static VAr compensator

The presented SVC includes an SCR-controlled shunt reactor and a parallel connected capacitor (see Fig. 12) [6, 10, 11]. The simulation results for the combined system with an SVC are shown in Figs. 13 and 14. As shown, the voltage of the collection bus is depressed because the fault occurrence and the reactive power supplied by the SVC slowly increases to about 16MVAr and the responses differ between different turbine types. However, only the response of the type-B turbine is shown because it

Copyright © 2016 International Journal of Automation and Smart Technology

exhibits the lowest terminal voltage of all turbine types (Fig. 7(a).

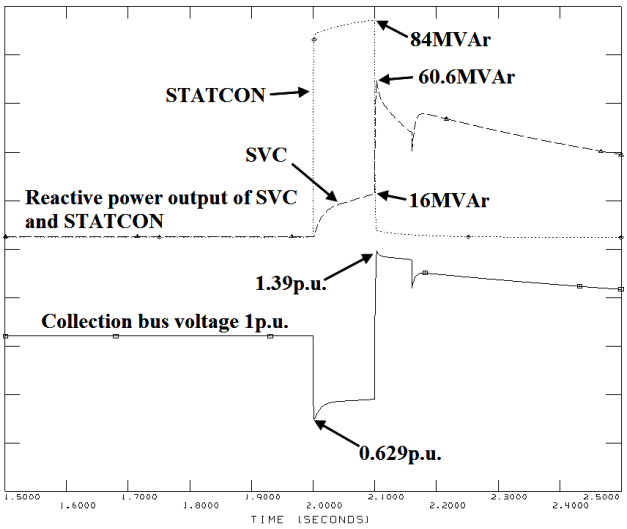

Figure 13. Simulation results of reactive power output and voltage responses of SVC and STATCON for fault on the grid of Peng-Hu.

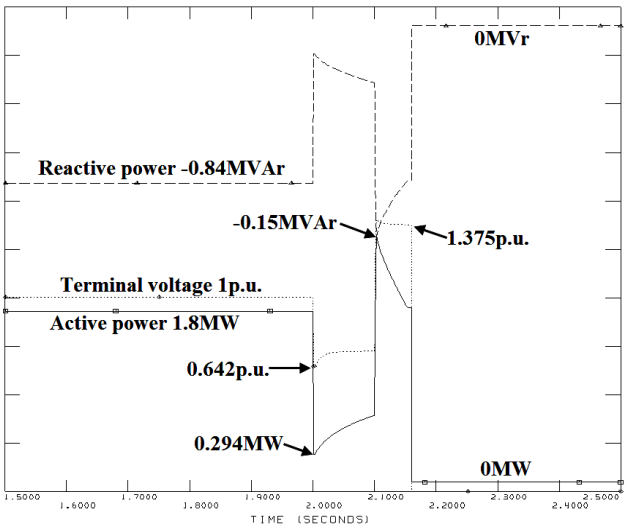

Figure 14. Terminal voltage and active and reactive power responses of the type-B wind turbine for fault on the grid of Peng-Hu with SVC operation.

Static synchronous compensator

A STATCOM is a voltage source converter (VSC) device (Fig. 15) [6]. The reactive power at the terminals of the STATCOM depends on the amplitude of the voltage source. For example, if the terminal voltage of the VSC is higher than the AC voltage at the point of connection, the STATCOM generates a reactive current; on the other hand, when the amplitude of the voltage source is lower than the AC voltage, it absorbs reactive power [6].

The presented STATCOM is assumed to not provide net exchange of active power with the network, and the DC capacitor remains charged at the desired level [12]. The simulation results of a STATCOM-integrated the wind farm are shown in Fig. 13. The internal voltage of the STATCOM is depressed when the fault occurs, and the reactive current is increased immediately [6]. It is notable that the STATCOM response time is much faster than that of an SVC, mainly because of the switching times provided by the IGBTs of the voltage source converter.

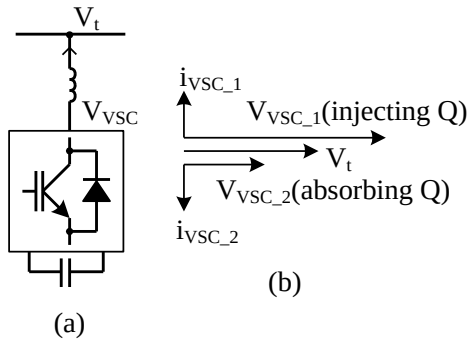

Figure 15. STATCOM arrangement (a) STATCON connection; (b) vector diagram.

Conclusion

This paper assesses the impact of an offshore wind farm interconnected into Taiwan's power grid. The wind farm includes three types of wind turbines (Types B, C and D). Simulation results show disturbance responses in the submarine cables connecting the wind farm to the grid are dependent on turbine type, specifically the turbine's fault ride through capability, which is associated with turbine performance dynamic system stability. Finally, the response time of reactive power compensation devices integrated in the wind farm is found to be an important factor for determining the farm's fault ride through capability.

Acknowledgment

This project was supported by Taiwan Power Company under Grant TPC-546-4102-9703.

References

[1] T. Ackermann, *Wind Power in Power Systems*. New Jersey, USA: John Wiley & Sons, 2005.

[2] A. Reidy and R. Watson, "Comparison of VSC based HVDC and HVAC Interconnections to a Large Offshore Wind Farm," in proceedings of *IEEE Power Engineering Society General Meeting*, San Francisco, CA, USA, Jun. 16, 2005, pp. 1-8. doi: 10.1109/PES.2005.1489081

[3] R. Rudervall, J. P. Charpentier, and R. Sharma, "High Voltage Direct Current (HVDC) Trans- mission Systems Technology Review Paper," in proceedings of *National Power Electronics Conference*, Xian, China, Sep. 23-26, 2006.

Copyright © 2016 International Journal of Automation and Smart Technology

[4] F. Schettler, H. Hung, and N. Christl, "HVDC Transmission System Using Voltage Sourced Converters Design and Applications," in proceedings of *IEEE PES Summer Meeting*, Seattle, WA, USA, Jul. 16-20, 2000, pp. 715-720. doi: 10.1109/PESS.2000.867439

[5] R. P. S. Leão, T. Degner, and F. L. M. Antunes, "An Overview on the Integration of Large-Scale Wind Power into the Electric Power System," Dep. Of Electrical Engineering, Federal University of Ceará, Brazil, 2007.

[6] A. L. Olimpo, J. Nick, E. Janaka, C. Phill, and H. Mike, *Wind Energy Generation: Modeling and Control*. New Jersey, USA: John Wiley & Sons, 2009.

[7] PSS/E-29, Power Technologies, Inc., October 2002.

[8] Wind Turbine Generator Models, *PSS/E Dynamic Models Documentation*, no. 3, 2004.

[9] G. Ramtharan, A. Arulampalam, J. B. Ekanayake, F. M. Hughes and N. Jenkins, "Fault Ride Through of Fully Rated Converter Wind Turbines with AC and DC Transmission Systems," *IET Renew. Power Gener.*, vol. 3, no. 4, pp. 426-438, 2009. doi: 10.1049/iet-rpg.2008.0018

[10] K. R. Padiyar, *Analysis of Subsynchronous Resonance in Power Systems.* Berlin, Germany: Springer Science & Business Media , 1999.

[11] PSS/E 29, Online Documentation, Application guide, vol. II, Chapter14.

[12] PSS/E 29, Online Documentation, Application guide, vol. II, Chapter20.

Copyright © 2016 International Journal of Automation and Smart Technology